高等学校化学学报
CHEMICAL JOURNAL OF CHINESE UNIVERSITIES
综合评述

含Si，P，B的非传统超支化发光聚合物研究进展

吴　锐，李　政，李　琪，石佳俊，赵　艳，冯维旭，颜红侠
（西北工业大学化学与化工学院，西安 710129）

摘要　综合评述了含Si、P、B的非传统超支化发光聚合物的最新研究进展. 此类发光材料通过Si-O-C、P-O-C、B-O-C等有机无机杂化单元构建成三维超支化拓扑结构，内部富含孤对电子的杂原子（如O、N、S）通过空间n/π相互作用、多重氢键网络及非金属配位键自发形成“簇发光中心”，并且具有优异的生物相容性，在药物控释可视化、细胞生物成像及高级信息加密等领域展现出巨大的应用潜力. 本文重点讨论了该发光材料的发光机理、结构-性能关系，并指出了当前面临的挑战与未来研究方向.

关键词　聚集诱导发光；聚合物；簇发光；超支化聚硅氧烷
中图分类号　O634　　**文献标志码**　A　　doi：10.7503/cjcu20250411

Recent Progress on Unconventional Hyperbranched Luminescent Polymers Containing Si，P and B

WU Rui，LI Zheng，LI Qi，SHI Jiajun，ZHAO Yan，FENG Weixu，YAN Hongxia*
（*School of Chemistry and Chemical Engineering*，*Northwestern Polytechnical University*，*Xi'an* 710129，*China*）

Abstract　This review summarizes recent advances in unconventional hyperbranched luminescent polymers containing Si，P，and B. These luminescent polymers form three-dimensional hyperbranched topological structures through organic-inorganic hybrid units such as Si-O-C，P-O-C，and B-O-C. Internally enriched with heteroatoms bearing lone pairs（*e.g.*，O，N，S），these heteroatoms spontaneously form clusteroluminogens through spatial n/π interactions，multiple hydrogen-bond networks and nonmetallic coordination bonds. Exhibiting excellent biocompatibility，these luminescent materials demonstrate significant application potential in fields such as drug-controlled-release visualization，cellular bioimaging，and advanced information encryption. We focus on discussing the luminescence mechanism and structure-property relationships of this luminescent material，while identifying current challenges and future research directions.

Keywords　Aggregation-induced emission；Polymer；Clusteroluminescence；Hyperbranched polysiloxane

1　Introduction

Rigid π-conjugated frameworks have long been regarded as essential structural elements for achieving highly efficient emission in organic/polymeric fluorescent materials，and have been successfully applied in fields such as organic light-emitting diodes（OLEDs），biological probes，and chemical sensing. However，the inherent rigid chain segments and low polarity characteristics of such systems pose challenges in dissolution

收稿日期：2025-12-30. 网络首发日期：2026-02-04.
联系人简介：颜红侠，女，博士，教授，主要从事有机无机杂化聚集诱导发光聚合物方面的研究. E-mail：hongxiayan@nwpu.edu.cn
基金项目：国家自然科学基金（批准号：22175143，22575194）资助.
Supported by the National Natural Science Foundation of China(Nos.22175143，22575194).

and processing. Strong π-π stacking between aromatic rings readily induces aggregation-caused quenching (ACQ), accompanied by potential phototoxicity and environmental persistence risks[1]. Therefore, developing a new generation of fluorescent materials that are "aromatic-free, heavy-metal-free, solution-processable, and exhibit enhanced luminescence in the aggregated state" has become a shared concern across chemistry, materials science, and life sciences. In 2001, Tang *et al.* first proposed the concept of aggregation-induced emission (AIE), overturning the traditional ACQ paradigm. This breakthrough provided novel insights for designing highly efficient solid-state luminescent materials and propelled a significant paradigm shift in luminescent materials research[2]. Over the past two decades, the AIE system has expanded from initial "propeller-type" small molecules like tetraphenylethylene and silole to a broad spectrum of materials including polymers, metal complexes, carbon dots, and metal nanoclusters[3—6]. From a mechanistic perspective, the Restriction of Intramolecular Motions (RIM) model is widely accepted. This theory posits that in aggregated states, intramolecular rotation/vibration is suppressed, blocking non-radiative transition pathways and forcing the release of excited-state energy in radiative form[7]. The establishment of the AIE mechanism not only expanded the structural boundaries of organic fluorescent molecules but also laid the theoretical and experimental foundation for subsequent exploration of non-conjugated luminescent systems[8].

However, the classic AIE system still relies on rigid π-conjugated units such as benzene rings as the luminescent core, and issues including phototoxicity, solubility, and environmental persistence remain unresolved[9—11]. Since 2013, a new class of luminescent materials——unconventional luminescent polymers, which abandon aromatic ring structures have entered the research community's focus. Typical examples include polyetheramine (PEA), polyethyleneimine (PEI), natural polysaccharides and proteins[12—15]. This phenomenon challenges the classical understanding that "conjugated structures are a prerequisite for luminescence," attracting widespread attention[16]. To explain its luminescent origin, Tang *et al.*[13] proposed the clusterization-triggered emission (CTE) mechanism in 2015. They suggested that the lone pair electrons (n electrons) carried by heteroatoms (O, N, S, etc.) within the material can interact with neighboring n electrons or π electrons through space interaction (through-space interaction, TSI), forming cluster luminescent centers. This interaction forms clusteroluminogens (CLgens), which then undergo radiative transitions to emit light. This phenomenon is termed clusteroluminescence[17]. This mechanism emphasizes the pivotal role of noncovalent interactions and spatial electron coupling in luminescence processes, extending the concept of luminescent centers from orbital conjugation to spatial conjugation. It provides a new paradigm for further expanding the theoretical framework of luminescence[18].

In 2015, the deep integration of siloxane chemistry with the AIE concept gave rise to a highly representative class of unconventional luminescent polymers——hyperbranched polysiloxanes (HBPSi)[19]. These macromolecules feature flexible Si-O-C backbones with side chains rich in alkoxy or hydroxyl groups. They can be efficiently synthesized *via* a one-pot transesterification-polycondensation reaction without metal catalysts or aromatic ring formation, with number-average molecular weights (M_n) controllable within the range of 3000—30000[20—24]. Its three-dimensional spherical topology not only endows the material with remarkable conformational freedom and surface functional group modifiability, but also provides abundant spatial electron coupling sites for the formation of electron-rich atom clusters, exhibiting typical AIE characteristics[25]. This system extends the concept of non-conjugated luminescence to inorganic-organic hybrid backbones incorporating inorganic molecules such as B and P, providing an expandable molecular platform for developing the next generation of cluster luminescent materials that are solution-processable, biocompatible, and environmentally friendly[26]. This review summarizes recent design, synthesis, structure-property relationships, and multidisciplinary applications of hyperbranched polymer luminescent clusters (Fig. 1). It

discusses current challenges and potential future research directions for hyperbranched polysiloxane luminescent materials. We hope this review will inspire new approaches for the precise construction and functional expansion of clusteroluminescence organic-inorganic hybrid materials.

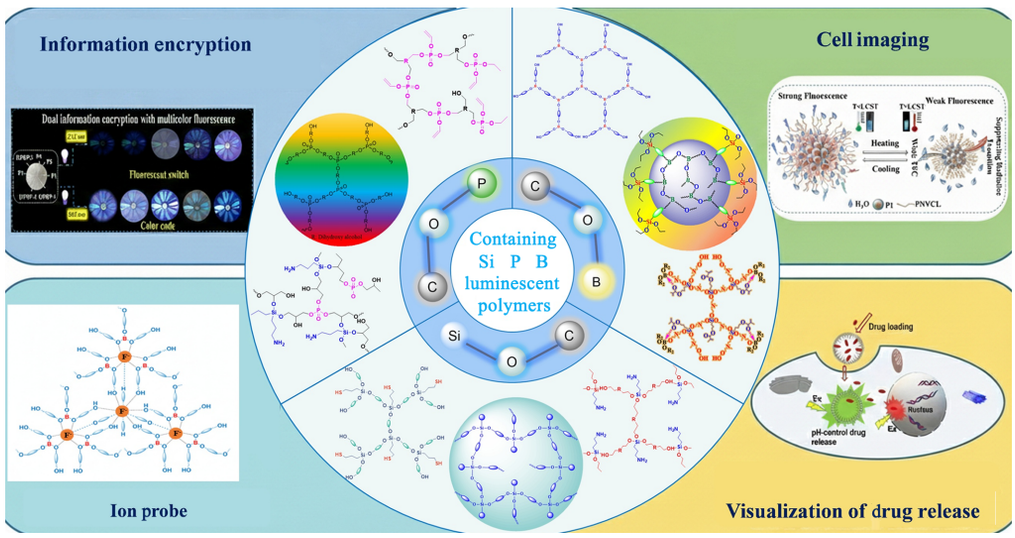

Fig. 1 Schematic diagram of the structure and applications of unconventional hyperbranched luminescent polymers containing Si, P, and B

2 Hyperbranched Polysiloxane

Yan's team[27] pioneered a catalyst-free, solvent-free transesterification polycondensation method, using siloxanes and diols as monomers to efficiently construct hyperbranched polysiloxanes with a Si—O—C backbone. This approach completely eliminates the reliance on precious metal catalysts such as Pt, Rh, Ir, and Ru in traditional silane addition reactions, while also avoiding the inherent drawbacks of hydrolysis-poly condensation processes, namely gelation susceptibility and difficulty in replication[28]. Featuring mild reaction conditions, high atom economy, and simple post-treatment, it provides a reproducible paradigm for the scaled-up synthesis and green manufacturing of HBPSi[20,29,30]. Structurally, the Si—O—C bond angle of approximately 120° lies between the flexible C—O—C (110°) and rigid Si—O—Si (130°) angles. This confers a unique conformation on the chain segment characterized by easy folding and difficult internal rotation. The flexibility ensures rapid aggregation of the chain segment in solution or bulk, while the rigidity suppresses non-radiative relaxation. This synergy enables HBPSi to exhibit intrinsic AIE behavior. Hyperbranched topology enables multiple Si—O units to pack densely at the nanoscale, forming compact CLgens. More importantly, the Si—O—C segments in HBPSi provide an ideal model system for CTE theory. Without relying on traditional π-conjugated structures, spatial interactions can form within the 0.10—0.32 nm scale solely through short-range spatial coupling between electron-rich atoms[8]. By systematically modifying cluster size, electron density, and microenvironmental polarity through strategies such as controlling diol chain length, introducing C=O/C=C local conjugated segments, and terminating with β-cyclodextrin or amino acids, the research team achieved continuous transitions from blue to red light, nanosecond to microsecond emission lifetimes, and single-emission to multicolor/multimode luminescence (including fluorescence and delayed fluorescence). This demonstrates the universality and designability of "clusterization-triggered emission" in non-conjugated polymers.

2.1 Pure *n*-electron System

Recently, Bai *et al.*[31] synthesized a series of blue-emitting HBPSi polymers——HBPSi-2C, HBPSi-3C,

HBPSi-4C, HBPSi-5C, and HBPSi-6C——*via* transesterification polycondensation reactions between (3-aminopropyl) triethoxysilane (APTES) and diols of varying chain lengths (C2—C6) (Fig. 2). The study revealed that the short-chain HBPSi-2C and HBPSi-3C exhibited significantly superior emission wavelength, luminous intensity, and fluorescence quantum yield (QY) compared to the longer-chain HBPSi derivatives. The study indicates that shorter chain lengths result in closer spacing between functional groups (—OH, —NH_2, —SiO_3), enabling hydrogen bonding and Si←N coordination to drive molecular aggregation into compact clusters. Electron cloud overlap within luminescent clusters induces spatial electron delocalization, whose scale expands as chain length decreases. This leads to narrowed highest occupied molecular orbital-lowest unoccupied molecular orbital (HOMO-LUMO) energy gap and reduced excited-state energy, resulting in red-shifted emission wavelengths, enhanced QY, and the manifestation of excitation-dependent and concentration-enhanced emission. Additionally, Yan *et al.*[32] designed and synthesized three terminally thiol-functionalized (—SH) HBPSis (HE, HP, HB), systematically investigating their luminescent properties. Among these, HP exhibited optimal blue light emission (480 nm) and QY (12.23%). The thiol and hydroxyl groups in HP establish dual hydrogen bonds (H···S/H···O) and O···O spatial interactions, promoting the clustering of electron-rich atoms like sulfur and oxygen into luminescent centers. This narrows the HOMO-LUMO energy gap, red-shifting the emission wavelength to 480 nm. The moderately long rigid carbon chain and flexible Si—O—C segments establish a "rigid-flexible synergistic effect" conformation equilibrium. This facilitates dense aggregation while restricting molecular motion and suppressing nonradiative transitions, thereby significantly enhancing luminescence intensity and QY.

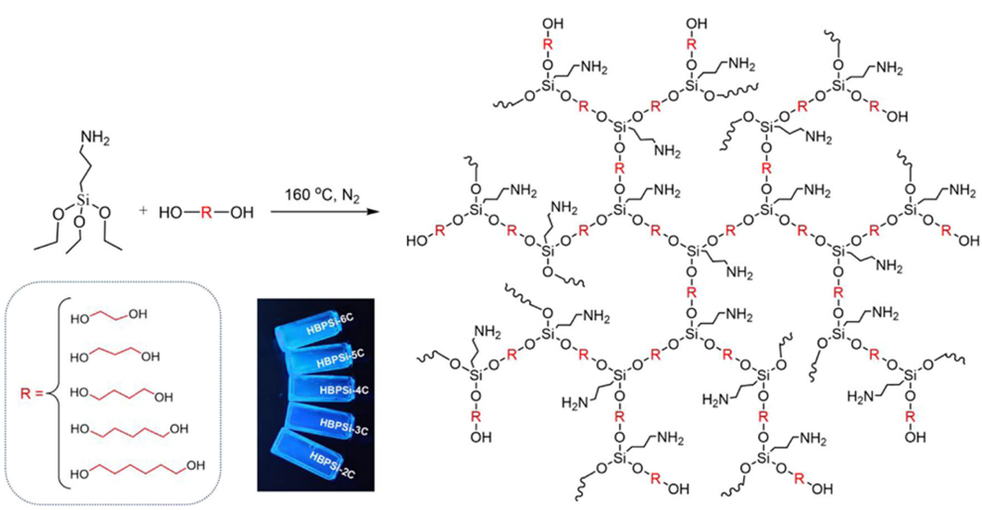

Fig. 2 Synthesis route of HBPSi-*n*C[31]

Copyright 2023, American Chemical Society.

This combination of rigidity and flexibility is also observed in polysiloxanes with other structures. Du *et al.*[33] pioneered the introduction of rigid piperazine units into the side chains of hyperbranched polysiloxanes, creating a class of highly efficient luminescent materials containing only *n* electrons. These materials exhibit a QY as high as 20.9%, which can reach 82.6% under pH regulation. The flexible Si-O segments in chains HBPSi-P1 and HBPSi-P2 bring N and O atoms into close proximity, forming pure *n*-electron clusters through multiple intermolecular hydrogen bonds. Concurrently, short-range O···O, N···N, and O···N interactions (0.25—0.31 nm) within the clusters establish spatial interactions. Rigid piperazine rings further restrict chain segment motion, suppressing non-radiative transitions. Under acidic conditions, protonation of tertiary/secondary amines induces charge repulsion, leading to a more rigid conformation and a dramatic increase in QY.

2.2 n/π Electron Hybrid Systems

Compared to pure non-conjugated systems, the introduction of n/π-mixed clusters generally results in red-shifted emission wavelengths, significantly enhanced QY, and prolonged excited-state lifetimes in AIE polymers[34—36]. Du *et al.*[37] synthesized four types of oligomers (HP1-HP4) [Fig. 3 (A)] by incorporating tertiary amines and C═C groups, which exhibited distinct fluorescent colors. Interestingly, pure HP1 containing C═C and tertiary amine emitted blue, green, and yellow fluorescence under various excitation lights, demonstrating color-tunable luminescence. Compared to HP3, which only contained C═C groups in the main chain, the optimal excitation/emission wavelengths of HP1 shifted to 520/550 nm and 525/554 nm in solution and in pure form, respectively. Experimental results and theoretical calculations indicate that the presence of tertiary amine and C═C groups enables efficient *n*-*n* and *n*-π spatial interactions, reducing the HOMO-LUMO gap of oligomers and facilitating excitation, thereby causing fluorescence red shift[Fig.3(B)].

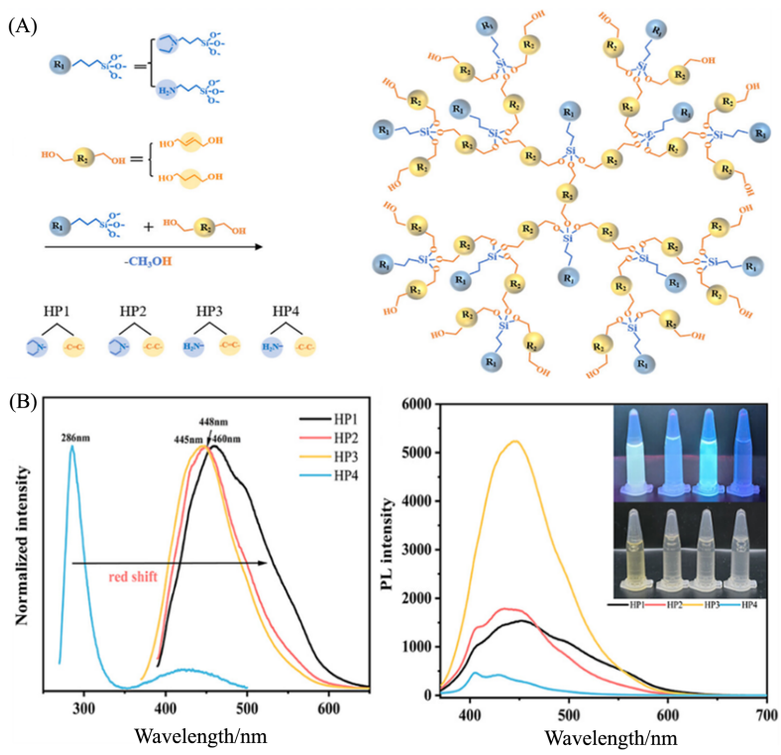

Fig. 3 Synthetic route of hyperbranched HP-1-4(A) and fluorescence emission spectrum of HP-1-4(B)[37]

Inset: images of HP1-HP4 solutions under 365 nm UV light.

n/π hybrid clusters can enhance QY. Reacting vinyl triethoxysilane (A-151) with 3,3′-dithiodipropionic acid (DTDP) yields HBPSi-A with a fluorescence QY of 47.8%[38]. Experimental and theoretical studies reveal that the high QY originates not from conventional conjugation but from disulfide-driven CLgens. The lone pair electrons of O and S form *n*-*n* and *n*-π spatial interactions with the carbonyl group and carbon-carbon double bond, while the increased dipole moment induces chain segment distortion. This promotes dense molecular aggregation within the highly branched topology. Within the aggregates, dual hydrogen bonds between H···O and H···S lock the conformation, forming rigid Clgens that significantly suppress nonradiative transitions induced by vibrational/rotational motions. This forces the release of excited-state energy primarily through radiative channels, thereby elevating the fluorescence QY to 47.8%.

Additionally, *n*-π and *n*-*n* spatial interactions can significantly increase the Stokes shift of polymers. Zhao *et al.*[39] synthesized three structurally similar but backbone-distinct hyperbranched poly-siloxanes *via* a

one-step transesterification polycondensation reaction [HBPSi-BDO (1, 4-butanediol), HBPSi-CYC (1, 4-cyclohexanediol), and HBPSi-CBD (*cis*-2-buten-1, 4-diol]](Fig.4). The planar vinyl groups in the backbone introduce rigidity by restricting segment rotation, synergistically forming dense clusters with electron-rich O/N atoms. Vinyl groups in the structure provide π electrons, which undergo spatial n-π interactions with n electrons, significantly reducing the HOMO-LUMO energy gap and enhancing the forbidden n-π^* transition. This synergistic effect lowers the excited-state energy and redshifts the emission wavelength to 484 nm, achieving an exceptionally large Stokes shift of 186 nm in a non-conjugated system. Subsequently, HBPSi-CBD was further conjugated with *L*-methionine to construct the functionalized material HBPSi-Met for ROS scavenging. The sulfide bond (—S—) in *L*-methionine can be oxidized by ROS to form a sulfoxide [—S(=O)—], exhibiting significant ROS scavenging capacity. Subsequently, Zhao *et al.*[40] proposed a novel strategy for tunable fluorescence properties by regulating electrostatic potential (ESP) polarization through unsaturation. The introduction of unsaturated structures such as alkyne groups increases π electrons, enriching electrons near the carbonyl oxygen atom and driving carbonyl clustering. Within the clustered region, enhanced n-π and n-n spatial interactions fostered spatial electron delocalization, narrowing the HOMO-LUMO energy gap while suppressing nonradiative transitions. This resulted in bright green emission at 512 nm with a QY of 29.6%, enabling concentration-dependent, tunable clusteroluminescence. This system was applied to an activation-type fluorescent diagnostic and therapeutic system for tumor-specific imaging and chemodynamic therapy (CDT). By forming a nanocomposite through coordination with Fe^{3+} and loading the hydrogen peroxide inhibitor AT, HBPSi-Fe^{3+} @AT was obtained. During this process, fluorescence is quenched by Fe^{3+} (OFF). Upon entering tumor cells, high GSH concentrations reduce Fe^{3+} to Fe^{2+}, restoring fluorescence (ON). Concurrently, Fe^{2+} catalyzes H_2O_2 to generate ·OH radicals, enabling CDT.

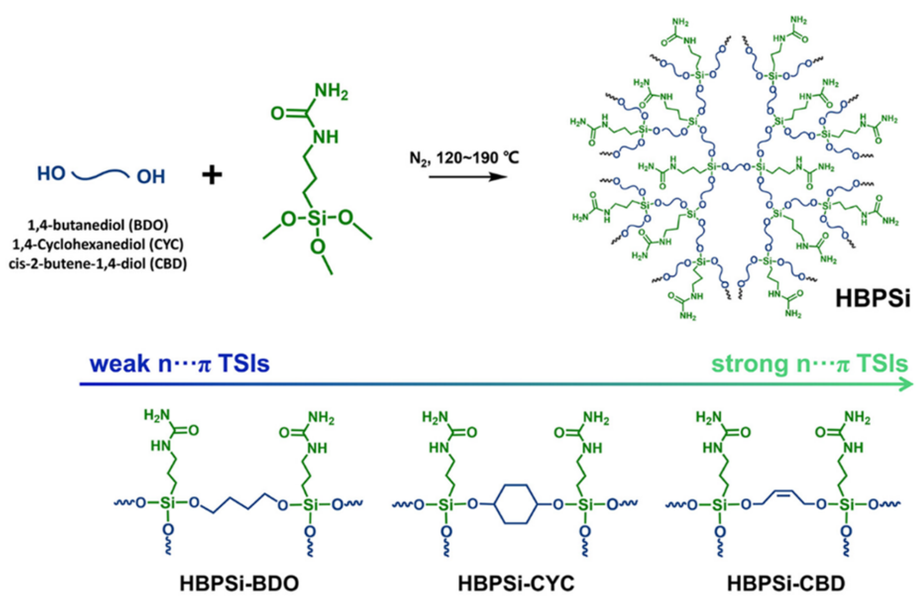

Fig. 4 Synthesis routes of HBPSi-BDO, HBPSi-CY and HBPSi-CBD[39]

Copyright 2024, American Chemical Society.

Yan *et al.*[41] introduced an imine bond (—N=C—) by reacting APTES with acetone *via* a Schiff base reaction. The transesterification polycondensation reaction with *N*-methyldiethanolamine(*N*-MDEA) constructed a hyperbranched structure (HBPSi-N). Experimental and theoretical studies revealed that HBPSi-N's red emission and millisecond-scale fluorescence lifetime stem from a rigid cluster structure synergistically formed by the imine bond, N/O heteroatoms, and terminal hydroxyl groups. The imine bond provides local

planar conjugation, while the heteroatom lone pair electrons form delocalized cluster states through multiple spatial interactions including N⋯H and O⋯H hydrogen bonds, as well as *n*-*n* and *n*-π interactions. This simultaneously narrows the HOMO-LUMO energy gap to achieve 620 nm red emission and suppresses nonradiative transitions. Concurrently, the spatial separation of HOMO-LUMO induces a twisted intramolecular charge transfer (TICT) effect with a ΔE_{ST} of only 0.086 eV, enabling T_1 excitons to return to S_1 *via* the RISC pathway. This confers an exceptionally long luminescence lifetime of 11.40 ms to the material.

2.3 Terminal Modification

By introducing terminal units with varying rigidity, polarity, or π-electron density, the intermolecular distance, hydrogen bond strength, and electron cloud overlap can be precisely tuned. This enables scaling up or down of the cluster state dimensions, achieving integrated enhancements in emission wavelength, QY, and functionality. Bai *et al.*[42] constructed hyperbranched polysiloxanes (HBPSi-2C-5C) by copolymerizing diols (C2-C5) with varying chain lengths and APTES. Through amidation reactions, three aromatic amino acids (Phe, Tyr, Trp) were introduced. The π-conjugated structures of these aromatic amino acids interact with electron-rich atoms (N, O, Si) in the polymer chain *via* hydrogen bonds, Si←N coordination, and *n*-π and *n*-*n* spatial interactions, forming dense clusters that establish a spatially delocalized electronic network. The HOMO predominantly distributes across amino groups, hydroxyl groups, Si-O clusters, and π bonds. The LUMO comprises π^* bonds and spatially delocalized states. As the π system expands, the band gap narrows and emission redshifts. Chain length modulates the rigid-flexible balance, with optimal matching (HBPSi-3C-Trp) yielding the densest cluster state and maximum electron cloud overlap, resulting in intense deep red emission.

Yan *et al.*[43] performed a transesterification polycondensation reaction between APTES and 1,3-propanediol to obtain HBPSi-NH_2. β-Cyclodextrin (β-CD) was then covalently grafted onto HBPSi-NH_2 to yield HBPSi-β-CD. Terminal modification with β-CD elevated luminescence performance from weak blue to full-spectrum high brightness. The rigid β-CD macrocycle enhanced hydrogen bonding and intermolecular interactions, promoting the formation of pure *n*-electron clusters of varying sizes. Overlapping O and N electron clouds within clusters created spatial delocalization, causing the bandgap to continuously narrow with increasing aggregation. Emission shifted from blue to red. Rigid β-CD suppresses chain motion, reduces non-radiative losses, and achieves QY exceeding 40% across all bands, enabling excitation-dependent high-brightness multicolor CLgens. Subsequently, APTES underwent transesterification polycondensation with diethylene glycol to yield HBPSi. Oleic acid (OA) at varying concentrations was grafted onto HBPSi *via* amide bonds to produce HBPSi-OA1 to OA4[44]. OA provided long hydrophobic segments, promoting tighter molecular aggregation. The C═C double bonds in OA contributed π orbitals, forming *n*-π spatial interactions with *n* electrons. DFT calculations revealed that the HOMO-LUMO energy gap of HBPSi-OA was lower than that of HBPSi, facilitating easier excitation. Furthermore, OA forms the surface layer while HBPSi constitutes the core, creating a hydrophobic core-hydrophilic shell supramolecular structure. This promotes larger cluster states, weakens non-radiative processes, increases QY from 23% to 28%, and exhibits AIEE and fluorescent resonance energy transfer (FRET) energy transfer, achieving high-brightness multicolor luminescence in a purely non-conjugated system. Zhao *et al.*[30] introduced electron-rich atoms into the polymer backbone by reacting APTES with diethylamine, then amide-grafted *L*-cysteine (—SH, —CONH—) to construct a donor-silicon bridge-acceptor D-A type structure (HBPSi-Cys). Subsequently, the AS1411 aptamer was linked *via* a disulfide bond to yield the tumor-targeting probe HBPSi-Apt. In dilute solutions, it exhibits localized excitation (LE) emission at 424 nm; in polar solvents or aggregated states, it displays TICT emission at 500 nm, with intensity significantly enhanced upon aggregation. Within the HBPSi-Cys non-conjugated

backbone, —OH/—NH donors and —SH/—CONH— acceptors form D-A pairs *via* spatial proximity of Si—O—C segments. Under polar conditions, molecular distortion occurs, enabling charge transfer *via* spatial coupling across the silicon bridge to the acceptor, yielding 500 nm TICT emission. In the aggregated state, multiple O⋯O/N hydrogen bonds induce electron cloud overlap, constructing a spatially delocalized and rigidified framework that suppresses nonradiative transitions while reducing the energy gap. The AIE effect amplifies the weak TICT emission, ultimately achieving dual-color fluorescence.

3 Hyperbranched Polyphosphate

The n electrons in heteroatoms and the π electrons in unsaturated units constitute the fundamental building blocks of unconventional fluorescent polymers. Effectively regulating the interactions between n electrons and π electrons is crucial for enhancing fluorescence performance and understanding emission mechanisms[15]. Phosphorus in polymers commonly exists as phosphates (P—O), phosphonates (P=O), or phosphonamides (P—N). The P=O bond provides a strong π electron cloud, while the phosphorus atom itself possesses lone pair electrons. These n/π electrons serve as a key source of clusteroluminescence in unconventional luminescence. In the aggregated state, the P=O bond undergoes spatial overlap with the n/π electrons of neighboring O/N/S atoms, forming through-space conjugation (TSC). This reduces the bandgap and enables visible-to-near-infrared emission[10].

Phosphorus polymers primarily encompass polyphosphate esters and poly (phosphoramidites). Considering the electron-rich nature of phosphorus atoms and the excellent biocompatibility of phosphates[45], Yan *et al.*[46] synthesized a novel non-aromatic AIE polymer, hyperbranched poly(phosphoramidite) (PPA), in 2021. PPA was synthesized *via* a green, one-pot ester-amine reaction between triethyl phosphate and ethylenediamine (PPA1) or 1,6-hexanediamine (PPA2). PPA is a viscous liquid appearing pale yellow under sunlight but emits intense fluorescence under 365 nm UV light. PPA1 exhibits optimal excitation at 399 nm and optimal emission at 443 nm. Following excitation at 399 nm, the experimentally measured fluorescence lifetime for PPA1 is 1.28 ns with a QY of 21.08%, while PPA2 demonstrates a QY of 26.93%. The fluorescence of PPA is attributed to the formation of luminescent clusters and electron transfer induced by spatial conjugation. The longer chain in PPA2 enhances the flexibility of the PPA2 molecule, leading to the formation of denser luminescent clusters. Notably, PPA exhibits sensitivity to Cu^{2+}, capable of converting the color of $CuCl_2$ solution from colorless to purple, thereby providing a convenient visual indicator for Cu^{2+} detection.

Polyphosphate esters simultaneously contain abundant lone pair electrons and π electrons, which can promote electron charge transfer and generate long-wavelength emission. Bai *et al.*[47] designed and synthesized a series of novel hyperbranched polyphosphate esters with distinct structures. The QY of HPPE1, HPPE2, and HPPE3 excited at 400 nm were 12%, 10%, and 3%, respectively. Theoretical calculations indicate that HPPE molecules aggregate due to strong intermolecular/intramolecular hydrogen bonding, forming distinct aggregates in solutions of varying concentrations. Subsequently, hydroxyl and $OP(O)_3$ groups aggregate and function as luminescent centers. Additionally, the balance between polymer stiffness and flexibility enhances luminescence. Interestingly, HPPE-doped PVA films exhibit blue room-temperature phosphorescence due to increased stiffness. Bai *et al.*[48] synthesized a series of aliphatic oligomeric polyphosphate esters rich in n- and π-electrons [Fig.5(A)]. These polymers emit radiation ranging from blue to deep red under different excitations. The fluorescence of these aliphatic oligomeric polyphosphate esters originates from intramolecular/intermolecular n-π spatial interactions, heteroatoms rich in lone pairs (O, N, P) form dense clusters with π-type groups (P=O) driven by hydrogen bonding, delocalizing electron clouds to act as emission centers. Polymerization and aggregation further concentrate negative charges and narrow the

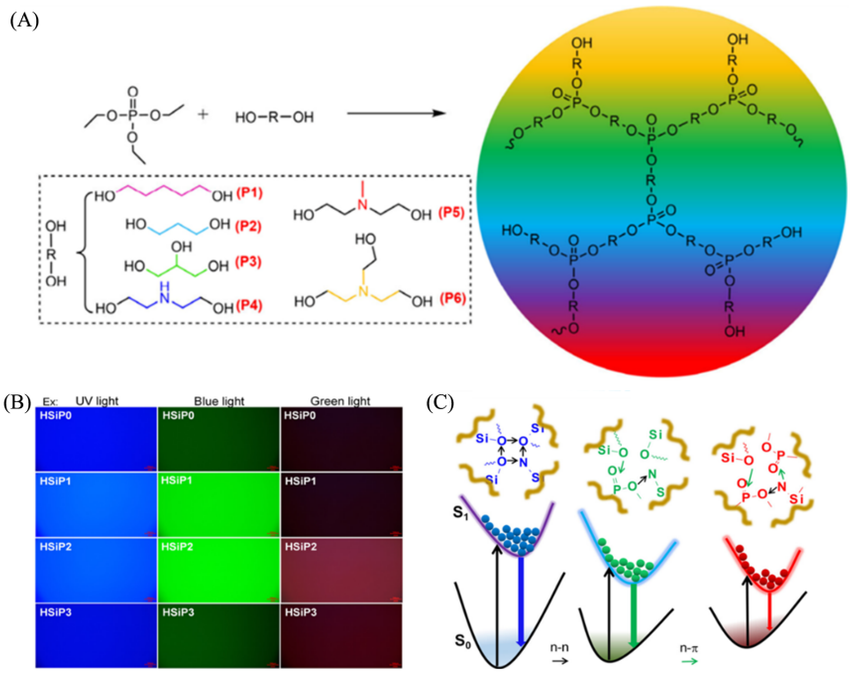

Fig. 5 Synthesis route of hyperbranched polyphosphate(A)[48], multicolor emission of HSiP0, HSiP1, HSiP2, and HSiP3(B) and potential energy surfaces for the emission from the enhanced spatial electronic communication(C)[49]

(A) Copyright 2025, American Chemical Society; (B, C) copyright 2025, American Chemical Society.

HOMO-LUMO energy gap, leading to increased fluorescence intensity with concentration and wavelength red-shift, ultimately achieving deep red emission without any aromatic rings. Additionally, these polymers hold potential for application in preparing fluorescent hydrogels. In 2025, Bai *et al.*[49] synthesized four hyperbranched poly(silicon phosphates)(HSiP0—HSiP3). Experimental results demonstrated that increasing the P═O(O)$_3$/Si(O)$_3$ ratio yields stronger red fluorescence[Fig.5(B)]. Enhanced *n*-π interactions between P═O and O/N atoms in the polymer structure promote negative charge concentration and spatial electron communication, thereby narrowing the bandgap and generating intense red emission. Concurrently, functional group clusters attract negative charges from isolated functional groups, further intensifying fluorescence [Fig.5(C)].

4 Hyperbranched Polyborosiloxanes

Boron (B), as the sole nonmetallic element in the third main group (III A), has an atomic number of 5 and a ground-state electron configuration of $1s^2 2s^2 2p^1$. Its 2*p* orbital contains only a single electron, resulting in a pronounced electron-deficient character. This vacant orbital endows the boron center with exceptional electron-accepting capability, enabling the formation of extended intramolecular charge transfer (ICT) pathways through *p*-π or *n*-*p* conjugation with neighboring electron-rich groups. In recent years, researchers have leveraged this property to embed boron atoms into polycyclic aromatic hydrocarbons or boron-containing π-conjugated frameworks, constructing a series of boron-containing fused-ring fluorescent materials. Among these, the B←N coordinate bond-driven rigidification strategy can significantly enhance the radiative transition rate constant, achieving high-intensity emission covering the entire visible spectrum with a photoluminescence QY far exceeding that of traditional aromatic fluorophores. However, such boron-containing polycyclic compounds generally rely on extended π-conjugated planes, making it difficult to meet the stringent low-toxicity requirements for *in vivo* imaging and diagnostic/therapeutic applications[50]. More

challenging still, boron-containing fluorescent polymers that completely eliminate aromatic rings to circumvent toxicity remain rarely reported: on one hand, saturated segments fail to provide effective conjugated pathways, and the large energy gap (ΔE>3.5 eV) in boron-centered n-σ transitions causes excitation energy to dissipate predominantly through nonradiative processes; On the other hand, B—O or B—N bonds readily undergo reversible hydrolysis and alcoholysis in aqueous environments, causing quenching of the luminescent centers and structural collapse of the material. Therefore, the core scientific challenge in developing next-generation biocompatible boron-containing fluorescent polymers lies in activating the boron center's radiative pathway through spatial electron coupling or CTE mechanisms while simultaneously suppressing hydrolytic toxicity *via* chemical modification, without incorporating aromatic rings[51].

In 2022, Yan *et al.*[52] synthesized three hyperbranched polyborate polymers (HBPB-1—HBPB-3) using tri-*n*-butyl borate (TBB) and various diols (1,3-propanediol, 1,4-butanediol, and 1,5-pentanediol) as reactants *via* transesterification polycondensation [Fig. 6(A)]. Among these, HBPB-2 exhibited a high QY of 54.1%, rivaling some aromatic fluorescent polymers. Theoretical calculations revealed that the rigid BO_3 planes in the hyperbranched borate polymer HBPB-2 structure restrict intramolecular rotation and vibration, while the flexible aliphatic carbon chains promote the aggregation of luminescent clusters. This "rigid-flexible synergistic effect" facilitates the aggregation of luminescent clusters in HBPB-2 while simultaneously suppressing non-radiative transitions to a certain extent [Fig. 6(B)]. Furthermore, driven by intermolecular hydrogen bonding, the O atom with a lone pair forms a B←O spatial coordination bond with the electron-deficient B atom, further stabilizing the aggregate structure.

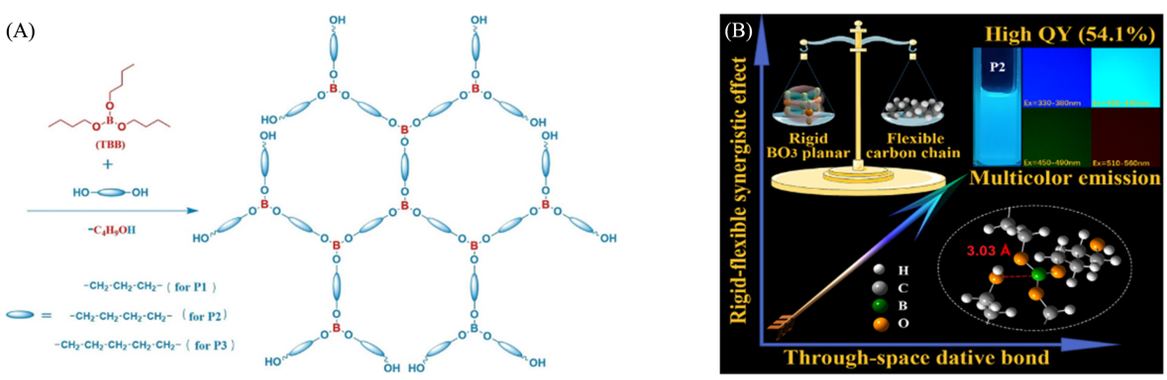

Fig. 6 Synthesis routes of the HBPB-1—HBPB-3(A) and illustration of intrachain interactions for HBPB-2(B)[52]
Copyright 2022, Wiley-VCH.

The optimal emission of the above three HBPB polymers all falls within the blue to blue-green light region, with fluorescence lifetimes in the nanosecond range. To enhance the emission wavelength and fluorescence lifetime of hyperbranched polyborate, Yan *et al.*[53] in 2023 successfully red-shifted HBPB's fluorescence wavelength into the red region by grafting silane groups onto the polyborate surface, extending the fluorescence lifetime from the nanosecond to the microsecond range. A novel HBPB system was constructed by transesterification polycondensation of tributyl borate with aliphatic diols of varying charge densities (1,5-pentanediol, diethylene glycol, diethylamine, and *N*-methyldiethylamine). Further surface modification with ethyl orthosilicate yielded four hyperbranched polybromosiloxanes (HBPB-Si). Notably, HBPB-Si-4 exhibits red light emission at 640 nm with a luminescence lifetime of 9.73 μs. Theoretical analysis indicates significant intermolecular forces exist within these polymer molecules, including multiple interactions such as Si—O···H, B—O···H, and C—H···O. Among these, HBPB-Si-4, characterized by higher electron density, exhibits reduced energy gaps and enhanced molecular conformation rigidity due to intramolecular hydrogen bonds and spatial interactions such as O···O and O···N. This configuration facilitates red emission.

Solvent-soluble, fully tunable luminescent materials have garnered significant attention for their ability to directly reveal solvent-luminescent group interaction mechanisms in the excited state. Yan *et al.*[54] successfully synthesized two hyperbranched polybromosiloxanes (HBPSi-B-1 and HBPSi-B-2) [Fig.7(A)], containing characteristic chemical bonds (B←N and B←C═O). Among these, HBPSi-B-1, exhibiting a typical D-π-A structure, emits red fluorescence at 645 nm with a quantum yield of 9.15%. This phenomenon originates from the synergistic effects of *n*-π and *n*-*n* spatial interactions induced by the B←N bond. The study revealed that solvent regulation enables continuous tuning of the emission wavelength of HBPSi-B-1 within the range of 418—588 nm, with HBPSi-B-2 exhibiting similar solvent-responsive characteristics. ESP analysis indicates that, beyond solvent polarity, the electronic effects play a crucial role in regulating the luminescence wavelength. When using acetylacetone (Hacac) as the solvent, the surface electrostatic potential distribution of HBPSi-B-1 becomes more balanced. Compared to the ethanol system and the solvent-free state, Hacac induces the formation of intramolecular O···O interactions and C—H···O hydrogen bond networks, confirming that increased solvent-molecule ESP differences enhance intramolecular interactions[Fig.7(B)]. These findings establish a novel fluorescence regulation mechanism based on the solvent electronic effect-electrostatic potential equilibrium-intramolecular interaction enhancement pathway. Leveraging the exceptional biocompatibility and fluorescent properties of polybromosiloxanes, Yan *et al.*[55] synthesized a thermosensitive polybromosiloxane using N-MDEA and APTES as reacting monomers. Through transesteri-fication polycondensation, they synthesized hyperbranched polysiloxane ($HBPSi\text{-}NH_2$) with terminal —OH and —NH_2 groups, grafted TBB onto its ends, and designed water-soluble hyperbranched polyborosiloxane (HBPSi-B-3). Subsequently, polyvinylcaprolactam (PNVCL) with thermosensitive properties was grafted onto the HBPSi-B-3 end groups *via* a Schiff base reaction, yielding the hyperbranched polyborsiloxane HBPSi-B-PNVCL containing thermosensitive segments. HBPSi-B-PNVCL exhibits not only bright red fluorescence at 627 nm with excitation-dependent characteristics but also possesses abundant O and N lone pair electrons and functional groups such as C═O and C═N. It self-assembles into rigid nanoclusters through intramolecular/intermolecular hydrogen bonding interactions with *n*-*n* and *n*-π spatial interactions. These cluster structures

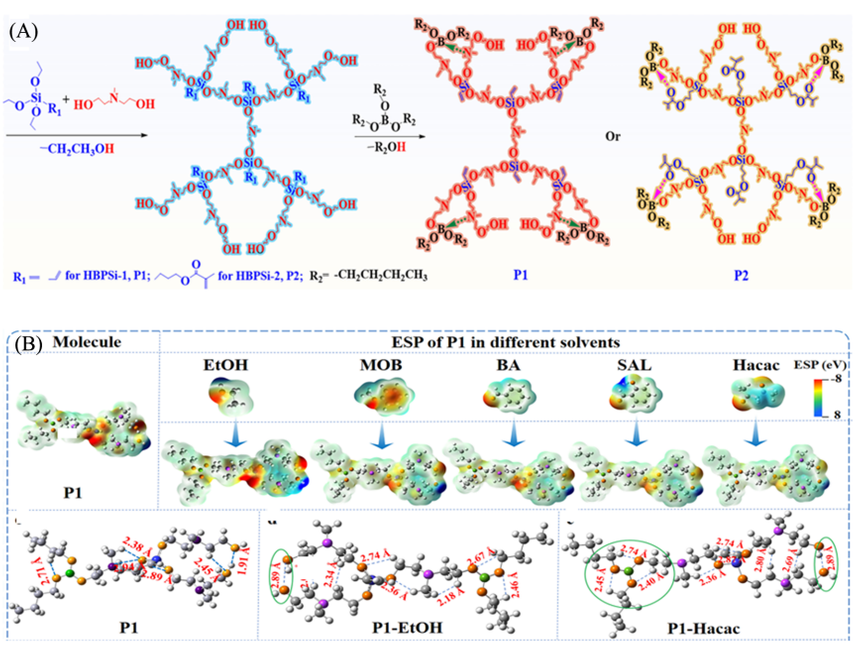

Fig. 7 Synthesis routes of HBPSi-B-1 and HBPSi-B-2(A) and ESP analysis of HBPSi-B-1(B)[54]

Copyright 2024, Wiley-VCH.

enable efficient radiative emission of $n\rightarrow\pi$ and $n\rightarrow\sigma$ transitions *via* TSC. The introduction of PNVCL further enhances molecular rigidity, suppresses non-radiative decay, and increases the QY to 5.95%.

5 Applications

Unconventional hyperbranched luminescent polymers containing Si, P, and B exhibit exceptional biocompatibility, tunable multicolor fluorescence emission, and stimulus-responsive properties due to their unique hyperbranched topological structure, heteroatom-induced spatial electron delocalization effects, and the TSC mechanism. These characteristics confer significant application potential in biomedical fields such as ion probe, information encryption and anti-counterfeiting, cell imaging, and controlled drug delivery.

5.1 Cation Detection and Anion Probes

The fluorescence emission of Si-, B-, and P-containing hyperbranched polymers originates from luminescent clusters formed by the aggregation of electron-rich atoms. When these clusters interact with electron-deficient species, they readily undergo through-space charge transfer (TSCT), thereby exhibiting significant stimulus-responsive characteristics. Based on this mechanism, such polymers have enabled the highly sensitive and selective detection of various metal ions, including Fe^{3+}, Mn^{2+}, and Co^{2+}. For instance, HBPSi-N, possessing lone pair electrons on the nitrogen atom within its imine bond (—N═C—), can coordinate with or conjugate to various metal ions to form stable complexes[41]. The addition of Mn^{2+} quenches over 90% of HBPSi-N's fluorescence intensity. The presence of other ions does not significantly affect the quenching effect of Mn^{2+} [Fig. 8(A)]. Further studies investigated the impact of varying Mn^{2+} concentrations on HBPSi-N. When the Mn^{2+} concentration ranges from 10 to 500 μmol/L, the fluorescence quenching rate of HBPSi-N

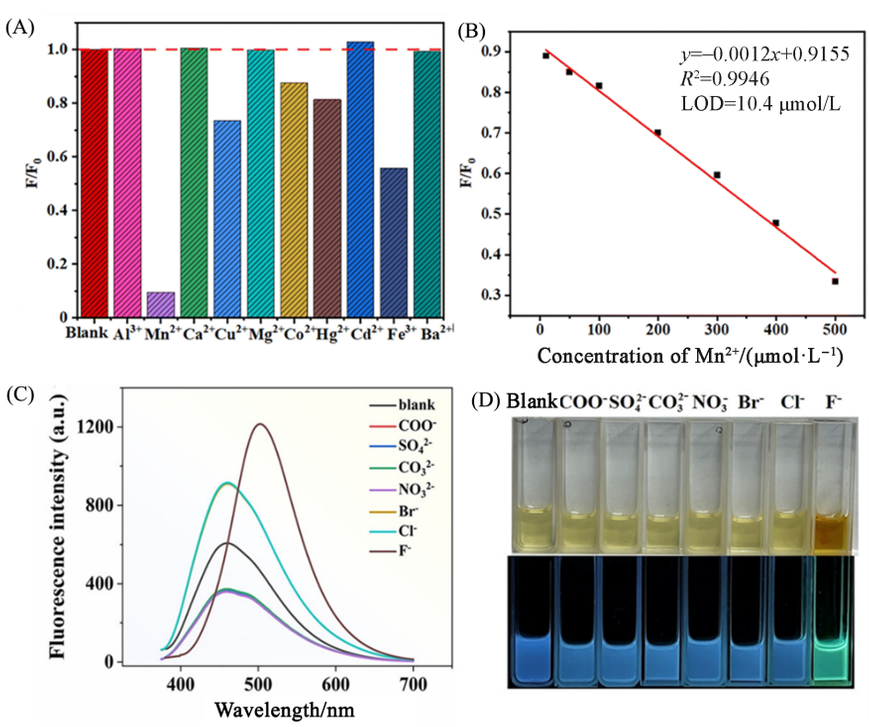

Fig. 8 The influence of different metal ions on the fluorescence intensity of HBPSi-N ethanol solution (20 mg/mL)(A), the linear relationship between the fluorescence intensity of HBPSi-N ethanol solution and the concentration of Mn^{2+} ions(B)[41], the selectivity and anti-interference tests of HBPSi-B-1(C) and fluorescence photos with different anions(D)[54]

(A, B) Copyright 2025, the Royal Society of Chemistry; (C, D) copyright 2024, Wiley-VCH.

exhibits a good linear relationship with its concentration. At 20 mg/mL, the detection limit is 10.40 μmol/L [Fig.8(B)]. The boron-containing system(HBPSi-B-1) utilizes the Lewis acidity of boron atoms to form B←F bonds with strongly Lewis-basic F^- ions[54], inducing fluorescence enhancement and red shift[Fig.8(C)]. This enables highly selective bright green fluorescence detection of F^- ions[Fig.8(D)].

5.2 Information Encryption and Anti-counterfeiting

Unlike traditional single-wavelength luminescent materials, unconventional polymers exhibit pronounced concentration-dependent luminescence and excitation wavelength dependence, enabling advanced encryption. Based on the fluorescence quenching effect of Fe^{3+} on HBPSi-C and the protection-recovery mechanism of Na_2EDTA, a dual-mode information encryption system was constructed[56]. During the encryption stage, "AIE 20th" was written on HBPSi-C-coated security paper using an aqueous Na_2EDTA solution as invisible ink, rendering the recorded content invisible under both daylight and UV irradiation. For decryption, $FeCl_3$ solution was applied as a "key", and under 365 nm UV excitation, the Na_2EDTA-protected regions exhibited blue fluorescence while the unprotected regions appeared dark due to Fe^{3+}-induced quenching, thereby enabling visual readout of the information [Fig.9(A)]. This process achieves high-security information protection without altering the macroscopic appearance of the paper. Leveraging HBPSi-Tyr's long-wavelength fluorescence properties, an information encryption application has been developed[57]. HBPSi-Tyr solutions enable blue fluorescent fingerprint imaging on qualitative filter paper. Under 365 nm UV light, secondary details such as bifurcation points, central points, and terminal points are clearly visible, with high contrast between dark ridge valleys and fluorescent ridges [Fig.9(B)]. This effect arises from the polymer's preferential adhesion to fingerprint ridges.

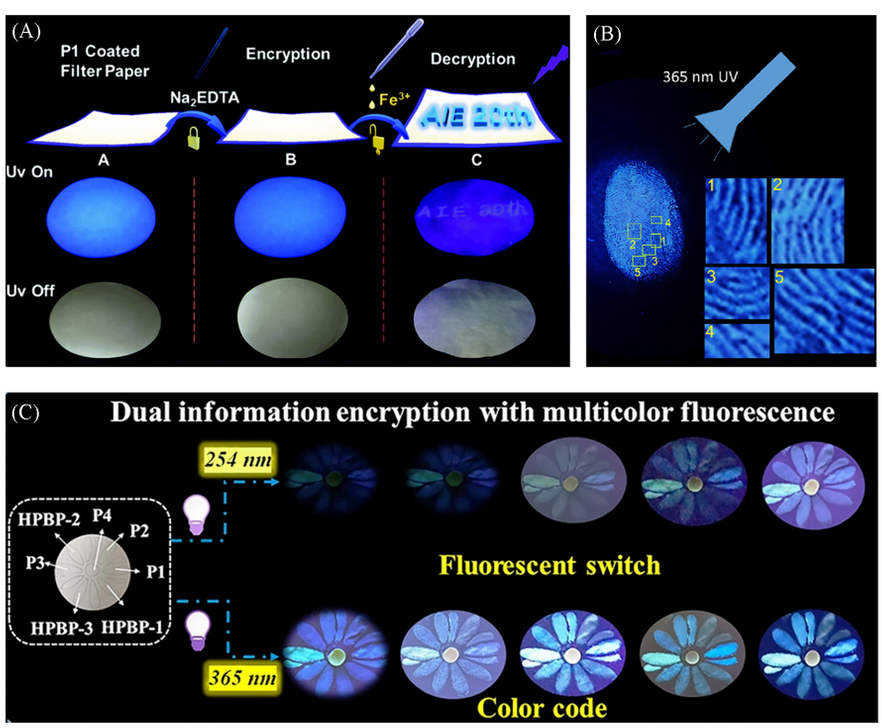

Fig. 9 HBPSi-C for information encryption and decryption(A)[56], fluorescence imaging of a latent fingerprint (bifurcation point, end point, and center point) on qualitative filter paper under excitation of 365 nm of UV light by HBPSi-Tyr(B)[57], and photographs of dual information encryption(C)[53]

(A) Copyright 2020, the Royal Society of Chemistry; (B) copyright 2022, American Chemical Society; (C) copyright 2023, Wiley-VCH.

Additionally, seven distinct fluorescent materials [HBPB-(1—3) and HBPB-Si-(1—4)] were used to prepare fluorescent inks, which were applied to filter paper to form "flower" patterns [Fig. 9(C)][53]. Dual encryption was achieved by adjusting ink concentration and excitation wavelength. Under 254 nm UV light, increasing concentration only enhances fluorescence intensity (intensity encryption), making color distinctions difficult to the naked eye. However, under 365 nm excitation, both intensity enhancement and a distinct red shift occur simultaneously, causing the pattern to exhibit a noticeable color shift from blue to red (color coding). This combined strategy of "fluorescent switching" and "color coding" significantly enhances the contrast, signal clarity, and security of information encryption compared to single-intensity changes, offering new insights for advanced anti-counterfeiting applications.

5.3 Visualization of Drug Release and Cell Imaging

HBPSi materials demonstrate multifunctional integration potential in biological systems due to their excellent water solubility and biocompatibility. HBPSi-β-CD utilizes the cavities of surface β-CD to encapsulate hydrophobic drugs such as ibuprofen. Drug loading capacity increases with drug concentration, reaching up to 160 mg/g (approaching saturation at drug concentrations ≥2 mg/mL, Fig. 10(A)[43]. Its drug release exhibits pronounced pH responsiveness, under weakly acidic conditions (pH=6.4), cumulative release reaches 78% within 24 h; whereas in neutral conditions (pH=7.4), only 35% is released within 6 h, with subsequent release ceasing almost entirely [Fig. 10(B)][43]. This discrepancy stems from altered electrostatic interactions between the carrier and drug, under acidic conditions, both the carrier (containing amine groups) and the drug (containing carboxyl groups) carry positive charges, inducing electrostatic repulsion that promotes drug release; under neutral conditions, the positively charged carrier and negatively charged drug undergo electrostatic attraction, inhibiting drug release. Therefore, HBPSi-β-CD can serve as a pH-responsive controlled-release carrier for targeted delivery of hydrophobic drugs and enable visualization of the drug release process.

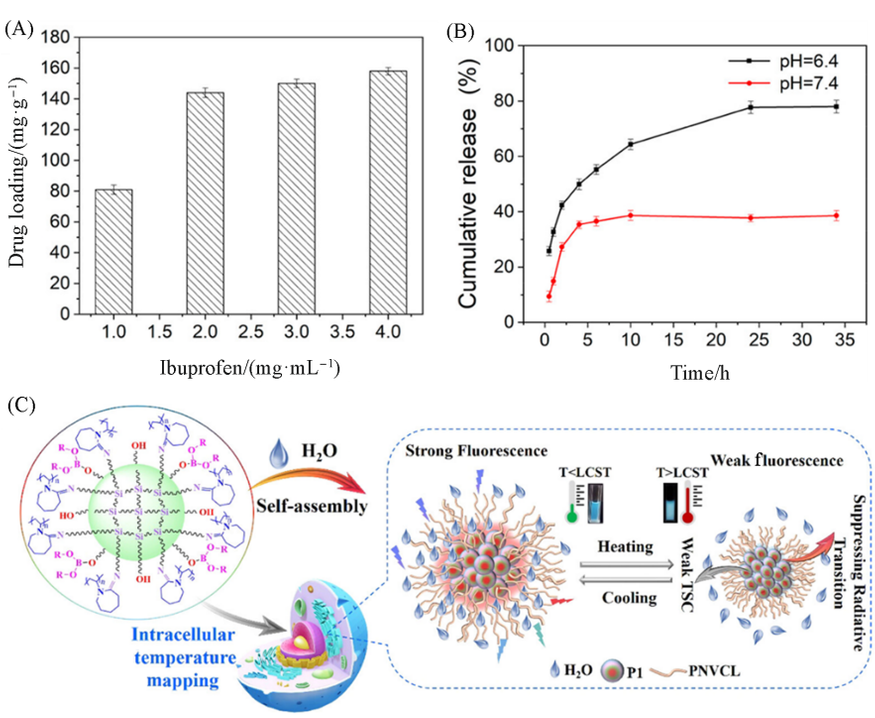

Fig. 10 Drug loading(A) and release(B) of HBPSi-β-CD[43] and schematic of the mechanism for HBPSi-B-PNVCL's temperature-induced fluorescence intensity decrease(C)[55]

(A, B) Copyright 2022, American Chemical Society; (C) copyright 2025, American Chemical Society.

Specifically, observations at different temperatures (31, 38 and 41 ℃) reveal that as temperature increases, the fluorescence intensity of HBPSi-B-PNVCL significantly decreases and its color changes: yellow-green at 31 ℃(strong red/green/blue channels), blue-green at 38 ℃(weakened red channel), and a faint blue-violet hue at 41 ℃(with significant reduction in red/green channels). This temperature-dependent color shift enables real-time visualization of temperature changes within living cells, indicating the potential application of HBPSi-B-PNVCL for intracellular temperature mapping[Fig.10(C)][55].

6 Summary and Outlook

Currently, over 70 intramolecular organic-inorganic hybrid luminescent polymers have been synthesized by modulating Si-O-C, B-O-C, and P-O-C backbone structures and terminal functional groups. These include polysiloxanes with multicolor fluorescence, polyborates with high QY (up to 54.1%) and polyborosiloxanes with long-lifetime fluorescence (9.73 μs). Although the non-aromatic skeleton in polymers endows it with unique performance advantages, it inevitably leads to an inherent limitation of low fluorescence quantum yield. Inspired by classical luminescence theory, the research team effectively suppressed nonradiative transitions through a rigidity-enhancing strategy—including the introduction of locally conjugated structures, β-cyclodextrin(β-CD), and B-O-C linkers—significantly boosting fluorescence efficiency. The HBPSi system exhibits a wide QY range (2.0%—47.8%). The introduction of local conjugation and β-CD markedly increased QY, with HBPSi-A and HBPSi-β-CD reaching up to 47.8% and 46.1%, respectively. Boron-containing hyperbranched polymers (HBPB/HBPB-Si) predominantly exhibit QY values between 2% and 15%. Notably, HBPB-2 achieves 54.1%, demonstrating quantum yields comparable to traditional aromatic ring polymers and revealing substantial potential for mechanism exploration. Phosphorus-containing hyperbranched polymers(HPPE) currently exhibit a maximum yield of approximately 26.9%, with significant room for further optimization. These materials have been successfully applied in ion detection, information encryption, cell imaging, visualization of controlled drug release, and functionalization of thermosetting resins.

However, such luminescent polymers still face the following scientific challenges: (1) currently developed intramolecular hybrid luminescent materials struggle to achieve both long wavelengths and high QY. Most reported high-quantum-yield intramolecular hybrid luminescent materials typically emit only blue fluorescence, with QY in the deep red/near-infrared region generally below 10%. Therefore, how can we overcome the limitations imposed by the energy gap law on non-radiative transition rates through aggregation state engineering(*e.g.*, heavy atom effects, exciton coupling) to maintain exciton radiative transition pathways dynamically? (2) The assembly kinetics of these organic-inorganic hybrid luminescent polymers are uncontrollable, limited by the poor cyclic stability of dynamic noncovalent bonds(hydrogen bonds), making it difficult to achieve stable arrangements of single chiral structures or specific emitters. Consequently, how can molecular design precisely regulate the kinetic pathways of supramolecular assembly to achieve a controlled thermodynamic-kinetic equilibrium? (3) The spatial conformation and electronic coupling strength of cluster luminescent centers in HBPSi luminescent materials are highly sensitive to molecular weight, branching degree, and terminal functional groups. This results in significant batch-to-batch variations in emission wavelength, QY, and lifetime, leading to insufficient reproducibility. (4) HBPSi exhibits relatively weak mechanical properties and thermal stability, with a glass transition temperature (T_g) typically below 0 ℃. This makes it difficult to meet the long-term service requirements of flexible optoelectronic devices in high-temperature and high-humidity environments. (5) The clusteroluminescence behavior of HBPSi is sensitive to water and oxygen. Prolonged storage or UV irradiation readily induces hydrolysis of Si—O—C bonds and

silanol condensation, leading to fluorescence decay. Therefore, achieving precise construction, performance tuning, and functional expansion of HBPSi cluster luminescent materials still requires systematic and in-depth research across multiple dimensions, including molecular design, aggregation state regulation, and interface engineering.

References

[1] Ma F. L., Zhang S. W., Jiang J. H., Liu Y., Sun J. W., Lam J. W. Y., Zhao Z., Tang B. Z., *Adv. Mater.*, **2024**, *37*, 2414188
[2] Ling Y., Liu X. J., Hao H. J., Hao X. H., Bai L. B., Wu Y. G., *Chem. J. Chinese Universities*, **2018**, *39*(6), 1319—1325
[3] Wu Z. N., Yao Q. F., Zang S. Q., Xie J. P., *Natl. Sci. Rev.*, **2021**, *8*(6), nwaa208
[4] Liu Y. Y., Zhang X., Li K., Peng Q. C., Qin Y. J., Hou H. W., Zang S. Q., Tang B. Z., *Angew. Chem. Int. Ed.*, **2021**, *60*(41), 22417—22423
[5] Yu M. X., Huang R. S., Guo J. J., Zhao Z. J., Tang B. Z., *PhotoniX*, **2020**, *1*(1), 1—32
[6] Duo Y. H., Han L., Yang Y. Q., Wang Z. F., Wang L. R., Chen J. Y., Xiang Z. Y., Yoon J. Y., Luo G. H., Tang B. Z., *Chem. Rev.*, **2024**, *124*(20), 11242—11347
[7] Tu Y., Zhao Z., Lam J. W. Y., *Natl. Sci. Rev.*, **2021**, *8*(6), nwaa260
[8] Hu R. R., Qin A. J., Tang B. Z., *Prog. Polym. Sci.*, **2020**, *100*, 101176
[9] Zhang Z. T., Xiong Z. P., Chu B., Zhang Z. M., Xie Y., Wang L., Sun J. Z., Zhang H. K., Zhang X. H., Tang B. Z., *Aggregate*, **2022**, *3*, e278
[10] Liu X., Chu B., Xiong Z. P., Liu B., Tu W. H., Zhang Z. T., Zhang H. K., Sun J. Z., Zhang X. H., Tang B. Z., *Mater. Horiz.*, **2024**, *11*, 1579—1587
[11] Wang Y. Y., Liu Z. A., Huang J. M., Wei H. L., Jiang C. J., Wei L. Z., Jiang B. L., Zou L. M., Xie H. H., Gong Y. Y., *Small*, **2025**, *21*, 2411123
[12] Tomalia D. A., Klajnert-Maculewicz B., Johnson K. A. M., Brinkman H. F., Janaszewska A., Hedstrand D. M., *Prog. Polym. Sci.*, **2019**, *90*, 35—117
[13] Chen X., Sun Y., Yuan W. Z., *Macromol. Chem. Phys.*, **2025**, *226*, 2400401
[14] Wang Z. Y., Zhang H. K., Li S. Q., Lei D. Y., Tang B. Z., Ye R. Q., *Top. Curr. Chem.*, **2021**, *379*(2), 14—36
[15] Zhang J. Y., Xiong Z. P., Zhang H. K., Tang B. Z., *Nat. Commun.*, **2025**, *16*(1), 3910
[16] Tang S. X., Yang T. J., Zhao Z. H., Zhu T. W., Zhang Q., Hou W. B. W., Yuan W. Z., *Chem. Soc. Rev.*, **2021**, *50*(22), 12616—12655
[17] Zhang H. K., Tang B. Z., *JACS Au*, **2021**, *1*(11), 1805—1814
[18] Xu L., *Coord. Chem. Rev.*, **2024**, *519*, 216094
[19] Niu S., Yan H. X., *Macromol. Rapid Commun.*, **2015**, *36*(8), 739—743
[20] Niu S., Yan H. X., Chen Z. Y., Yuan L. X., Liu T. Y., Liu C., *Macromol. Rapid Commun.*, **2016**, *37*, 136—142
[21] Niu S., Yan H. X., Chen Z. Y., Li S., Xu P. L., Zhi X. L., *Polym. Chem.*, **2016**, *7*, 3747—3755
[22] Niu S., Yan H. X., Li S., Xu P. L., Zhi X. L., Li T. T., *Macromol. Chem. Phys.*, **2016**, *217*(10), 1185—1190
[23] Niu S., Yan H. X., Chen Z. Y., Du Y. Q., Huang W., Bai L. H., Lv Q., *RSC Adv.*, **2016**, *6*(108), 106742—106753
[24] Niu S., Yan H. X., Li S., Tang C., Chen Z. Y., Zhi X. L., Xu P. L., *J. Mater. Chem. C*, **2016**, *4*(28), 6881—6893
[25] Zhao Z., Li A., Yuan W. Z., *Acc. Chem. Res.*, **2025**, *58*(4), 612—624
[26] Wu R., He Y. Y., Li Z., Yu Z. Y., Guo X., Yan H. X., *Chem. Eur. J.*, **2025**, *31*, e202501133
[27] Buonomo J. A., Eiden C. G., Aldrich C. C., *Synthesis*, **2018**, *50*, 278—281
[28] Hamada T., Sugimoto T., Maeda T., Katsura D., Susumu M., Ohshita J., *Langmuir*, **2022**, *38*, 5829—5837
[29] Feng Y. B., Bai T., Yan H. X., Ding F., Bai L. H., Feng W. X., *Macromolecules*, **2019**, *52*(8), 3075—3082
[30] Zhao Y., He M. M., Xu L., Zhang C., Guo L. L., Feng W. X., Yan H. X., *Biomacromolecules*, **2023**, *24*(4), 1888—1900
[31] Bai L. H., Liu X., Yan H. X., Zhao S. S., Han X., *Langmuir*, **2023**, *39*(34), 12053—12062
[32] Wu R., Lian S. X., He Y. Y., Li Z., Zhao Y., Feng W. X., Yan H. X., *J. Mater. Chem. B*, **2024**, *12*(41), 10584—10592
[33] Du Y. Q., Liu Y. W., Li J. W., He Y. Y., Li Y. B., Yan H. X., *Small*, **2023**, *19*(40), 2302095
[34] Wang L., Xiong Z. P., Sun J. Z., Huang F. H., Zhang H. K., Tang B. Z., *Angew. Chem. Int. Ed.*, **2024**, *136*(8), e202318245
[35] Ye S. Y., Bao Y. Y., *Chem. Mater.*, **2024**, *36*(12), 5878—5896
[36] Sakhno T. V., Sakhno Y. E., Kuchmiy S. Y., *Theor. Exp. Chem.*, **2023**, *59*(2), 75—106
[37] Yang Z. K., Du Y. Q., Li Q. W., Zhang J. Y., Li Q. L., Yan H. X., *Macromolecules*, **2025**, *58*(5), 2450—2458
[38] Bai T., Zhang Y. S., Wang L., Yan H. X., Zhou W. H., *Aggregate*, **2023**, *4*, e267
[39] Zhao Y., Xu L., Feng Z. X., Yin S., Feng W. X., Yan H. X., *Biomacromolecules*, **2024**, *25*(4), 2635—2644
[40] Zhao Y., Feng Z. X., He M. M., Wang X. Y., Feng W. X., Tian W., Yan H. X., *Chem. Sci.*, **2025**, *16*, 11077
[41] Li Q., Qiao Y. J., Li Z., Wu R., Zhang Y. K., Zhao Y., Tian W., Wang R. M., Feng W. X., Yan H. X., *J. Mater. Chem. B*, **2025**, *13*(37), 11687—11695

[42] Bai L. H., Li H. Y., Gao J. Y., Ma X. T., Liu X. R., Yan H. X., Zhao S. S., Yu C. X., Li J. M., *Chem. Eng. J.*, **2024**, *499*, 156253
[43] Bai L. H., Yang P. F., Guo L. L., Liu S. S., Yan H. X., *Biomacromolecules*, **2022**, *23*(3), 1041—1051
[44] Bai L. H., Yan H. X., Guo L. L., He M. M., Bai T., Yang P. F., *Macromol. Chem. Phys.*, **2021**, *222*(23), 2100283
[45] Todorova Z., Tumurbaatar O., Todorova J., Ugrinova I., Koseva N., *Eur. Polym. J.*, **2021**, *142*, 110151
[46] Guo L. L., Yan H. X., Wang L. L., Yang P. F., Yan L. R., Zhao Y., *Mater. Adv.*, **2021**, *2*(23), 7701—7708
[47] Bai L., Liu X. R., Yan H. X., Zhao S. S., *Polym. Chem.*, **2023**, *14*(30), 3501—3511
[48] Bai L. H., Ge X. Q., Zhao S. S., Yang H., Li J. M., Yan H. X., Liu X. R., *Macromolecules*, **2025**, *58*(15), 8458—8467
[49] Bai L. H., Ge X. Q., Zhao S. S., Yang H., Li J. M., Yan H. X., Liu X. R., *Macromolecules*, **2025**, *58*(2), 1038—1047
[50] Kwok R. T. K., Leung C. W. T., Lam J. W. Y., Tang B. Z., *Chem. Soc. Rev.*, **2015**, *44*(13), 4228—4238
[51] Grams R. J., Santos W. L., Scorei I. R., Abad-García A., Rosenblum C. A., Bita A., Cerecetto H., Viñas C., Soriano-Ursúa M. A., *Chem. Rev.*, **2024**, *124*, 2441—2511
[52] Guo L. L., Yan L. R., He Y. Y., Feng W. X., Zhao Y., Tang B. Z., Yan H. X., *Angew. Chem. Int. Ed.*, **2022**, *61*(29), e202204383
[53] He Y. Y., Feng W. X., Qiao Y. J., Tian Z. X. Tang B. Z., Yan H. X., *Angew. Chem. Int. Ed.*, **2023**, *62*(48), e202312571
[54] He Y. Y., Qiao Y. J., Li Z., Feng W. X., Zhao Y., Tian W., Tang B. Z., Yan H. X., *Angew. Chem. Int. Ed.*, **2024**, *63*, e202413425
[55] He Y. Y., Wu R., Li Z., Zhang Y. K., Liu W. Y., Feng W. X., Yan H. X., *Biomacromolecules*, **2025**, *26*(5), 3011—3020
[56] Feng Y. B., Yan H. X., Ding F., Bai T., Nie Y. F., Zhao Y., Feng W. X., Tang B. Z., *Mater. Chem. Front.*, **2020**, *4*, 1375—1382
[57] Bai L. H., Zhang Y. Z., Yan H. X., Liu X. R., *Biomacromolecules*, **2022**, *23*(11), 4617—4628

(Ed.: H, K, M)